J. Ocean Univ. China (Oceanic and Coastal Sea Research)
https://doi.org/10.1007/s11802-018-3461-6
ISSN 1672-5182, 2018 17 (1): 53-64
http://www.ouc.edu.cn/xbywb/
E-mail:xbywb@ouc.edu.cn

Numerical Simulation of Mechanical Compaction of Deepwater Shallow Sediments

SUN Jin[1), *], WU Shiguo[1), 2), 3)], DENG Jingen[4)], LIN Hai[5)], ZHANG Hanyu[1)], WANG Jiliang[1)], and GAO Jinwei[1)]

1) *Laboratory of Marine Geophysics & Geo-Resources*, *Institute of Deep-Sea Science and Engineering*, *Chinese Academy of Sciences*, *Sanya* 572000, *China*
2) *Qingdao National Laboratory for Marine Science and Technology*, *Qingdao* 266237, *China*
3) *College of Earth Sciences*, *University of Chinese Academy of Sciences*, *Beijing* 100049, *China*
4) *State Key Laboratory of Petroleum Resources and Prospecting*, *China University of Petroleum*, *Beijing* 102249, *China*
5) *CNOOC China Limited Tianjin Branch*, *Tianjin* 300451, *China*

(Received March 1, 2017; revised May 3, 2017; accepted July 4, 2017)

Abstract To study the compaction law and overpressure evolution in deepwater shallow sediments, a large-strain compaction model that considers material nonlinearity and moving boundary is formulated. The model considers the dependence of permeability and material properties on void ratio. The modified Cam-Clay model is selected as the constitutive relations of the sediments, and the deactivation/reactivation method is used to capture the moving top surface during the deposition process. A one-dimensional model is used to study the compaction law of the shallow sediments. Results show that the settlement of the shallow sediments is large under their own weight during compaction. The void ratio decreases strictly with burial depth and decreases more quickly near the seafloor than in the deeper layers. The generation of abnormal pressure in the shallow flow sands is closely related to the compaction law of shallow sediments. The two main factors that affect the generation of overpressure in the sands are deposition rate and permeability of overlying clay sediments. Overpressure increases with an increase in deposition rate and a decrease in the permeability of the overlying clay sediment. Moreover, an upper limit for the overpressure exists. A two-dimensional model is used to study the differential compaction of the shallow sediments. The pore pressure will still increase due to the inflow of the pore fluid from the neighboring clay sediment even though the deposition process is interrupted.

Key words mechanical compaction; deepwater shallow sediments; compaction law; shallow water flow; overpressure evolution

1 Introduction

With the growing demand for petroleum energy, the development of deepwater (water depth > 500 m) oil and gas resources in the South China Sea is becoming increasingly important. Several deepwater oil and gas fields (such as Lingshui17-2 and Liwan21-1) have been developed so far (Xie, 2014). However, this development also presents new challenges to the deepwater drilling program. One typical challenge is the engineering geological problems that frequently occur during drilling in a shallow formation (Haneberg *et al*., 2015; Gherasim *et al*., 2015). Shallow sediments usually have low strength, high water content, and large porosity due to a shallow burial depth (about a few hundred meters). This condition is unfavorable for borehole stability, wellhead stability, and well control (Skogdalen *et al*., 2011). Moreover, shallow gas and shallow water flow (SWF) may sometimes occur while drilling shallow formations at deepwater sites (Mallick and Dutta, 2002; Sun *et al*., 2014). SWF sands are un-consolidated and usually have high porosity and pore pressure. Consequently, overpressure fluid will flow into the borehole when the drilling fluid cannot balance the formation pressure in these sands. This condition may cause large and long-lasting uncontrolled flows, well damage, foundation failure, formation compaction, and damaged casing (Sun and Zhang, 2015). Particularly, eruptions from overpressured sands may result in seafloor craters, mounds, and cracks. Such shallow geological disasters are closely related to the physical and mechanical properties of shallow layers. Thus, a good understanding of the mechanical and physical properties of the shallow layers is of crucial importance before designing a deepwater drilling program.

The physical and mechanical properties of shallow sediments are controlled by the compaction law of shallow layers. Although the water depth in the deepwater regions is large, the effective overburden pressure of the sediments is not so large due to the existence of pore wa-

* Corresponding author. E-mail: sunjin@idsse.ac.cn

ter according to Terzaghi's effective stress principle. The formation temperature is also low due to the low temperature of deep sea water and shallow burial depth. Thus, purely mechanical compaction will prevail in the upper shallow layers. Chemical compaction (such as pressure solution and montmorillonite dehydration) is unlikely to happen. Disregarding chemical aspects, this paper will focus on the modeling of purely mechanical compaction.

Compaction occurs when accumulating sediments compact under their own weight or tectonic movement, expelling pore water in the process. This process is analogous to the process of soil consolidation and reduces porosity, thereby changing physical and mechanical properties. Two major methods are used to study the compaction law of sediments: experimental and theoretical methods. The main early studies of empirical compaction model (Athy, 1930; Hedberg, 1936) were derived from laboratory experiments and actual field data. The most commonly used compaction models in soil mechanics are based on the results of oedometric or uniaxial strain compaction tests of soils. These models are still widely used in geological engineering due to their simplicity. The sediment compaction theory is studied based on consolidation theory of soil. The process of one-dimensional consolidation was first investigated by Terzaghi. Biot (1941) extended Terzaghi's theory to a three-dimensional situation. However, permeability and compressibility are assumed to be constant in their theories. Davis and Raymond (1965) established a nonlinear compaction model considering a change in permeability and compressibility. Audet and Flower (1992) and Flower and Yang (1998) also proposed a nonlinear diffusion equation based on Athy's empirical law to describe the compaction law of sediments. They found that the ratio of flow rate to the deposition rate is the main governing factor of pore pressure generation. However, the theories are applicable only to situations in which geometry varies slightly. Some researchers recognized this limitation and developed finite strain consolidation theory. One-dimensional large strain consolidation theories were first proposed by Gibson *et al*. (1967) with the assumption of constant permeability and compressibility. Gibson's model can be more generally applied to solve problems with changing loads. Thus, many researchers conducted their work following Gibson's model. Carter *et al*. (1977) proposed a three-dimensional large-strain consolidation model for both elastic and elastoplastic material based on Eulerian description to predict the behavior of a foundation resting on saturated clay and developed the corresponding finite element code. Chopra and Dargush (1992) derived large-strain consolidation equations based on Lagrangian description. Xie and Leo (2004) derived a one-dimensional large-strain consolidation model for thick and thin soil layers, and comparisons between classical small strain theory and large strain theory are given in their study. To evaluate the influence of soil's weight on consolidation, Xie *et al*. (2014) proposed a large-strain consolidation model that considers the nonlinearity of permeability and compressibility. Kikinzon *et al*. (2015) used mixed finite elements to develop a two-dimensional compaction model for simulating fluid flow and compaction in sedimentation basins. Bachrach (2016) established a plastic model based on natural strain increment formulation to simulate the compaction of formation. Compaction is a dynamic process with moving boundary conditions. To deal with moving boundaries, Gibson (1958) developed a one-dimensional analytical consolidation model for a clay layer that increases in thickness with time. Bernaud *et al*. (2006) used the deactivation/reactivation method to simulate the one-dimensional progressive deposition process of sediments.

The compaction models based on linear small strain assumption are relatively mature. By contrast, few models consider the nonlinearity of geometry, material, and permeability simultaneously. The current nonlinear models are focused on geometrical nonlinearity. Although some models consider material nonlinearity, most of them are based on poroelasticity theory or phenomenological relationships between porosity and effective vertical stress. In this paper, we proposed a large deformation numerical compaction model based on the modified Cam-Clay model. Sediment density, permeability, and mechanical properties are dependent on deformation parameters during the compaction process. The dynamic deposition process is considered by using the deactivation/reactivation method. One objective of this paper is to study the compaction law of deepwater shallow sediments, especially the void ratio profile, which is a key parameter to predict the formation pressure and mechanical properties. A second objective is to improve the understanding of how abnormal fluid pore pressures occurs and the factors that cause these abnormal pressures in shallow sands, which is known as SWF geological disaster, during deepwater drilling.

2 Model Formulation

Fully saturated sediments consist of two phases: a solid phase (the soil skeleton) and a fluid phase (the pore water). The compaction behavior involves two mechanical effects. First, changes in pore pressure cause changes in effective stress, thereby affecting the response of the solids. Second, the fluid in a zone reacts to mechanical volume changes by a change in pore pressure. The coupled fluid-mechanical process is formulated within the framework of the quasi-static Biot theory. Governing equations include equilibrium equation, fluid flow equation, mass conservation equation, geometric equation, and constitutive equation. In the derivation, we have the following assumptions: 1) The formation is fully saturated and behaves as a Cam-Clay material. 2) The fluid in the formation is sea water, and the fluid flow confirms to Darcy's law. 3) The fluid and solid skeleton are incompressible. 4) Terzaghi's effective stress principle is used to calculate the effective stress.

The equilibrium equation has the form

$$\frac{\partial \sigma_{ij}}{\partial x_j} + \rho g_i = 0 , \tag{1}$$

where σ_{ij} is the total stress tensor; $\rho=(1-n)\rho_s+n\rho_w$ is the

bulk density of sediments; ρ_s and ρ_w are the densities of the solid and fluid phase, respectively; n is porosity; and g_i is the ith component of gravity acceleration.

On the basis of Terzaghi's effective stress principle, Eq. (1) can be rewritten as (Sun *et al*., 2015)

$$\frac{\partial(\delta_{ij}\sigma_{ij}^{'}-P)}{\partial x_j}+\rho g_i=0\,, \tag{2}$$

where δ_{ij} is the Kronecker delta, σ'_{ij} is the effective stress tensor, and P is the pore fluid pressure.

The sediment permeability is assumed to be isotropic, and Darcy's law is used to describe the fluid flow through the sediments

$$q_i=-\frac{k}{\mu}\frac{\partial}{\partial x_i}(P-\rho_w g x_i)\,, \tag{3}$$

where q_i is the flow rate tensor, k is the permeability, μ is the viscosity of pore water, ρ_w is the mass density of the fluid, g is the gravity acceleration, and x_i is the position vector.

The solid and fluid phases are assumed to be incompressible. Thus, the volume change of the sediment skeleton is equal to the volumetric difference of the fluid flow into and out of a material element. The mass conservation equation can be written as

$$-q_{i,i}+q_v=\alpha\frac{\partial\varepsilon_v}{\partial t}\,, \tag{4}$$

where $q_{i,i}$ is the derivative of q_i with respect to x_i, q_v is the volumetric fluid source intensity, α is the Biot's coefficient, and ε_v is the volumetric strain.

The strain rate is derived from the velocity gradient as follows:

$$\dot{\varepsilon}_{ij}=\frac{1}{2}\left(\frac{\partial\dot{u}_i}{\partial x_j}+\frac{\partial\dot{u}_j}{\partial x_i}\right), \tag{5}$$

where $\dot{\varepsilon}_{ij}$ is the strain rate tensor, $\dot{u}_i$ is the velocity tensor, and x_i is the position tensor.

The constitutive law is used to describe the relation between effective stresses and strains. With a large deformation, the constitutive law is written in the incremental form. For isotropic poroelasticity, the constitutive law is

$$\begin{aligned}\Delta\sigma_{ij}^{'}&=(K-\frac{2}{3}G)\Delta\varepsilon_v\delta_{ij}+2G\Delta\varepsilon_{ij}\\&=[(K-\frac{2}{3}G)\dot{\varepsilon}_v\delta_{ij}+2G\dot{\varepsilon}_{ij}]\Delta t\,,\end{aligned} \tag{6}$$

where K is the bulk modulus, G is the shear modulus, $\Delta\varepsilon_v$ is the incremental volumetric strain, $\Delta\varepsilon_{ij}$ is the incremental strain tensor, and Δt is the time step.

In actual, the elastic stress–strain relationship is not applicable to deepwater sediments. Large plastic deformation usually occurs during compaction. The modified Cam-Clay model is a hardening/softening elastoplastic model, and it includes a particular form of nonlinear elasticity, which can provide a better description of the deformation behavior of soft clay during compaction. The yield function of the modified Cam-Clay model has the form

$$f=q^2+M^2p(p-p_c)\,, \tag{7}$$

where $M=\dfrac{6\sin\varphi}{3-\sin\varphi}$, φ is the friction angle for triaxial compression tests, $p=-\sigma'_{ij}/3$ is the mean effective stress, $q=\sqrt{3J_2/2}$ is the deviatoric stress, J_2 is the second in variant of the effective deviatoric stress tensor, and p_c is the consolidation pressure.

We assumed that both plastic and elastic principal strain increment vectors are coaxial with the current principal stress vector. The generalized strain increments are then decomposed into elastic and plastic parts so that

$$\Delta\varepsilon_p=\Delta\varepsilon_p^e+\Delta\varepsilon_p^p\,, \tag{8}$$

$$\Delta\varepsilon_q=\Delta\varepsilon_q^e+\Delta\varepsilon_q^p\,, \tag{9}$$

where $\Delta\varepsilon_p$ is the volumetric strain increment, and $\Delta\varepsilon_q$ is the shear strain increment. Superscripts e and p denote the elastic and plastic strain increment, respectively.

The associated flow rule is used here. Thus, we have

$$\Delta\varepsilon_p^p=\lambda_1\frac{\partial f}{\partial p}\,, \tag{10}$$

$$\Delta\varepsilon_q^p=\lambda_1\frac{\partial f}{\partial q}\,, \tag{11}$$

where λ_1 is the plastic multiplier that is related to the stress level.

In the modified Cam-Clay model, the evolution parameter is the void ratio e. The solid particles are assumed to be incompressible. Thus, the incremental relation between ε_p and e is

$$\Delta\varepsilon_p=-\frac{\Delta e}{e+1}\,. \tag{12}$$

The incremental form of Hooke's law in terms of generalized stress and strains is

$$\Delta p=K\Delta\varepsilon_p^e\,, \tag{13}$$

$$\Delta q=3G\Delta\varepsilon_q^e\,. \tag{14}$$

K is updated to reflect a nonlinear law derived experimentally from isotropic compression tests. The typical relations between e and p in the semi-logarithmic plot are shown in Fig.1.

As shown in Fig.1, e decreases as the normal consolidation pressure p increases. The point moves along the normal consolidation line under the loading condition

$$e=e_1-\lambda\ln\frac{p}{p_1}\,, \tag{15}$$

where p_1 is the reference pressure, e_1 is the void ratio at p_1,

and λ is the slope of normal consolidation line.

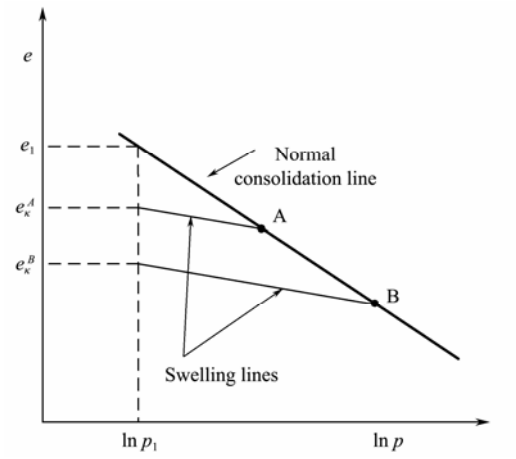

Fig.1 Relations of e–ln$p$ for an isotropic compression test.

Under the unloading condition (from point A or B on Fig.1), the point will move along an elastic swelling line of slope κ. The swelling line has the form

$$e = e_\kappa - \kappa \ln \frac{p}{p_1}, \tag{16}$$

where κ is the slope of the swelling line. The value of e_κ depends on the location of the point on the normal consolidation line from which unloading was performed.

The elastic part Δe^e can be obtained from the Taylor expansion of Eq. (16)

$$\Delta e^e = -\kappa \frac{\Delta p}{p}. \tag{17}$$

Dividing Eq. (17) by (1+e) gives

$$\Delta p = \frac{(1+e)p}{\kappa} \Delta \varepsilon_p^e = K \Delta \varepsilon_p^e, \tag{18}$$

From Eq. (17), we can conclude that the bulk modulus K increases as p increases, which means that the material is becoming more difficult to compress. This finding agrees with the actual experimental results.

From Fig.1, the plastic volumetric strain increment $\Delta \varepsilon_p^p$ can also be derived

$$\Delta \varepsilon_p^p = \frac{\lambda - \kappa}{1+e} \frac{\Delta p_c}{p_c}, \tag{19}$$

where p_c is the normal consolidation pressure. The plastic volume changes only when the normal consolidation pressure p_c changes.

Eq. (19) indicates that the consolidation pressure p_c varies with void ratio e and plastic volume increment $\Delta \varepsilon_p^p$, which will change the size of the yield surface. p_c should be updated in every step during the numerical calculation by using the formula

$$p_c = p_c^0 (1 + \frac{1+e}{\lambda - \kappa} \Delta \varepsilon_p^p), \tag{20}$$

where p_c^0 is the old consolidation pressure.

As the sediment is compacted, the void ratio decreases gradually, thereby affecting the permeability considerably. Nygård *et al*. (2004) found that the change in permeability during compaction of clays can be represented by the following equation:

$$k = k_0 \exp[b(e - e_0)], \tag{21}$$

where k_0 is the permeability of clay with void ratio e_0, and b is the permeability index, which usually varies from 3.66 to 9.70 for different clays.

Eqs. (1)–(21) describe the large deformation compaction of clay sediments. We will use these equations to solve the one- and two-dimensional compaction models in the following sections.

3 Numerical Implementation

Obtaining an analytical situation is impossible because of the strong nonlinearity of the problem and the moving boundary due to the dynamic deposition process. The numerical method is needed to solve the governing equations. FLAC^{3D} is an explicit finite difference program for rock and soil mechanical computation and is used here to implement the numerical calculation. FLAC^{3D} performs a Lagrangian analysis based on the time-marching scheme, which is suitable for large deformation and nonlinear analysis. However, considering the particularity of sediment compaction simulation, some challenges still need to be addressed.

3.1 Calculation of Void Ratio and Mass Density

In this paper, the one-dimensional compaction model is used to study the compaction law of deepwater shallow sediments. However, we should keep in mind that the one-dimensional compaction model is applicable only to the compaction of sediment basin with a large horizontal extent.

The mass density, permeability, and mechanical properties of sediments vary with the void ratio e. Unfortunately, e cannot be calculated automatically in FLAC^{3D} and is set to be constant as a type of physical property of the material. Thus, a fish function (an embedded programming language in FLAC^{3D}) is needed to calculate the void ratio during numerical simulation.

A schematic of deformation geometry of an infinitesimal body during one-dimensional compaction in the sediment is shown in Fig.2.

As shown in Fig.2, the current position h for a material point at position z at time t_0 is

$$h = z + u, \tag{22}$$

where u is the vertical displacement of the material point.

Before deformation, the volume of the infinitesimal body is An_0dz. When deformation occurs, the volume and the position of infinitesimal body change simultaneously. The change in volume is

$$\Delta V = A\mathrm{d}h = A\frac{\mathrm{d}h}{\mathrm{d}z}\mathrm{d}z\,, \tag{23}$$

where A is the cross section area of the sediment.

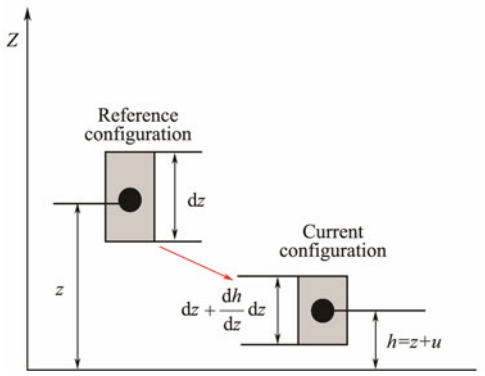

Fig.2 Schematic of deformation geometry of an infinitesimal body during one-dimensional compaction.

As the solid particle is incompressible, the change in volume is equal to the change in the void space. Therefore, the porosity at time t is

$$n(z) = \frac{A\mathrm{d}z n_0 + A\frac{\mathrm{d}h}{\mathrm{d}z}\mathrm{d}z}{A\mathrm{d}z + A\frac{\mathrm{d}h}{\mathrm{d}z}\mathrm{d}z} = \frac{n_0 + \frac{\mathrm{d}h}{\mathrm{d}z}}{1+\frac{\mathrm{d}h}{\mathrm{d}z}}, \tag{24}$$

where n_0 and $n(z)$ is the porosity of the same material point at time t_0 and t, respectively.

Substituting $n = \frac{e}{1+e}$ into Eq. (24) obtains

$$e = \frac{\mathrm{d}h}{\mathrm{d}z}(1+e_0) + e_0\,. \tag{25}$$

Under compaction, the solid particles become denser. Thus, the mass density of the sediments will change. This finding indicates that the mass density at each material point should be updated during numerical computation. Suppose that the dry mass density of the sediment at the initial state is ρ_{d0}, and the corresponding void ratio is e_0. ρ_d and e are the dry mass density and void ratio at time t, respectively. Given that the solid particles are not compressible, the volume of the solid phase V_s does not change. Therefore, we have

$$\rho_{d0} = \frac{\rho_s V_s}{V_0}, \rho_d = \frac{\rho_s V_s}{V}, \tag{26}$$

where ρ_s is the density of the solid phase, V_s is the volume of the solid phase, V_0 is the volume of the sediment skeleton at the initial state, and V is the volume of the sediment skeleton at time t.

According to Eq. (26), the ratio of ρ_d to ρ_{d0} is

$$\frac{\rho_d}{\rho_{d0}} = \frac{V_0}{V} = \frac{V_s(1+e_0)}{V_s(1+e)} = \frac{1+e_0}{1+e}\,. \tag{27}$$

Eq. (27) shows that the dry density varies with the void ratio. The dry density needs to be updated at every calculation step.

The resulting mass density is

$$\rho = \rho_{d0}\frac{1+e_0}{1+e} + \rho_w\frac{e}{1+e}\,. \tag{28}$$

3.2 Fluid–Mechanic Interaction Mode

The compaction behavior involves two mechanical effects. First, changes in pore pressure cause changes in effective stress, thereby affecting the response of the solids. Second, the pore fluid flow is induced due to mechanical volume changes. The mechanical response and the fluid flow have different time scales. Thus, we should choose the interaction mode of the solid and fluid phases. In the actual calculation, we set the mechanical module as the slave that must perform some sub-cycles (until the equilibrium state is reached in every step) for each flow fluid step. This situation means that we assume that the mechanical module can reach the equilibrium state instantaneously during each fluid step.

3.3 Method to Deal with the Moving Top Surface of Sediments

The characteristic of compaction simulation is that the calculation domain is an open system due to the continuous deposition of sediments. Gibson (1958) regarded the thickness of layer as a function of time to consider the moving boundary. Fowler and Yang (1998) developed a nonlinear diffusion equation to evaluate the influence of sedimentation rate on overpressure evolution with consideration of the dynamic deposition process. However, these methods are applicable only to the simple compaction model. Here we use Bernaud's (2006) method to deal with the moving top surface of sediments. This method is called the deactivation/reactivation method and is used frequently to simulate tunnel excavation and support.

The sediments that undergo compaction are modeled as a horizontal infinite layer, as shown in Fig.3.

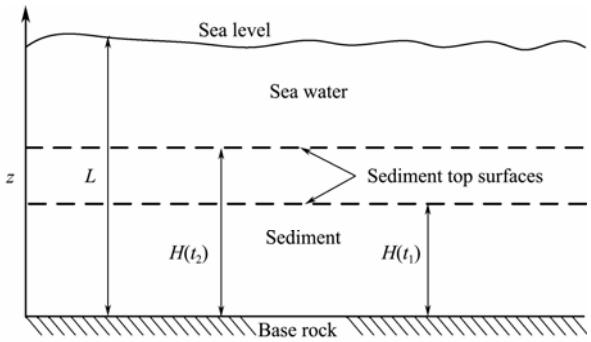

Fig.3 Schematic geometry of sediment.

The base rock is located at $z=0$. The mean distance between water level and the base rock is L. The thickness of sediment is H, and because of the continuous supply of sediments, the top surface of sediment changes with time. The boundary conditions are $\sigma_{zz} = \rho_w g[L-H(t)]$ and P

$=\rho_w g[L-H(t)]$ MPa at $z=H(t)$, and $u=0, \frac{\partial P}{\partial z}=-\rho_w g$ at $z=0$ (for impermeable case).

If we assume that the deposition rate is $\dot{m}$, then we can deduce that the velocity of top surface is

$$\dot{H}(t)=\dot{m}+\dot{u}\,, \tag{29}$$

where $\dot{H}(t)$ is the change rate of the top surface, $\dot{m}$ is the deposition rate, and $\dot{u}$ is the velocity of the sediment skeleton.

From Eq. (29), we can obtain the current position of the sediment top surface

$$H(t)=H(t-\Delta t)+\dot{m}\Delta t+\dot{u}\Delta t\,. \tag{30}$$

With the use of Eq. (30), the position of the moving boundary can be located in real time. However, this process requires mesh regeneration of the domain in real time and is very time consuming. The deactivation/reactivation method can overcome this difficulty efficiently. The method used here is similar to Bernaud's method and is illustrated as follows:

1) The geometric domain is discretized into n layers, which are called 'zones' in FLAC^{3D}. The thickness of each subdomain is set to be Δz.

2) At the initial state, the mass density of the domain is set to be equal to the sea water. The initial stress is set to be the hydrostatic pressure.

3) As time passes, $\dot{m}\Delta t$ is calculated during each time step. If $\dot{m}\Delta t<\Delta z$, then the new layer is not activated, and the corresponding mechanical properties do not change. Unlike in Bernaud's method, we will not change the permeability to a larger value because doing so will cause the time step to become too small. An alternative method is to shut down the fluid flow calculation in the unactivated layers in FLAC^{3D} to ensure that the pore pressure is unchanged. These settings ensure that only rigid movement occurs in the unactivated layers. If $\dot{m}\Delta t\geq\Delta z$, then a new layer has been added to the existing sediment. Then, the layer is activated and the corresponding mechanical properties are changed to the actual properties of the sediment. In addition, the void ratio and permeability are assigned to the new layers to execute the fluid flow calculation.

The dynamic deposition process can be simulated by implementing the above procedure. The boundary conditions will still hold, and the overlying unactivated layers behave similar to sea water.

4 Model Verification

For verification and comparison, the problem of one-dimensional consolidation of soil with initial thickness of H(m) is analyzed, in which a constant surface load is applied on the top surface instantaneously. The material is assumed to be homogeneous and behaves elastically. The fluid flow is described by Darcy's law. The analytical solutions of this one-dimensional consolidation problem were derived by Detournay and Cheng (1993), thus providing a reliable reference for validating the numerical method.

The diffusion equation for the pore pressure P is

$$\frac{\partial P}{\partial t}-\frac{k}{\mu S}\frac{\partial^2 P}{\partial z^2}=-\frac{\alpha}{(K+4G/3)S}\frac{d\sigma_{zz}}{\mathrm{d}t}\,, \tag{31}$$

where $S=\dfrac{\alpha^2}{K+4G/3}$ is the storage coefficient, and σ_{zz} is the total stress.

The boundary conditions are $\sigma_{zz}=p$ MPa and $P=0$ MPa at $z=H$, and $u=0, \dfrac{\partial P}{\partial z}=0$ at $z=0$.

The analytical solution for the pore pressure P is

$$P=\frac{2\alpha p_0}{(K+4G/3)S}\sum_{m=0}^{\infty}\frac{\sin(a_m\bar{z})}{a_m}\mathrm{e}^{-a_m^2\bar{t}}\,, \tag{32}$$

where $a_m=\pi(2m+1)/2$, $\bar{z}=\dfrac{H-z}{H}$, $\bar{t}=\dfrac{kt}{\mu SH^2}$.

The vertical displacement u has the form

$$u=\frac{2\alpha^2 Hp_0}{(K+4G/3)^2 S}\sum_{m=0}^{\infty}\frac{\cos(a_m\bar{z})}{a_m^2}\mathrm{e}^{-a_m^2\bar{t}}+\bar{z}-1\,. \tag{33}$$

The soil is discretized into 50 zones in the numerical calculation. The parameters needed for calculation are as follows: $H=50$ m, $p_0=1$ MPa, $K=0.5$ GPa, $G=0.2$ GPa, $\alpha=1$, $k=1\mathrm{e}^{-13}$ m^2, $\mu=1$ mPa.s. A comparison of pore pressure and displacement between the analytical and numerical solutions are shown in Figs.4 and 5.

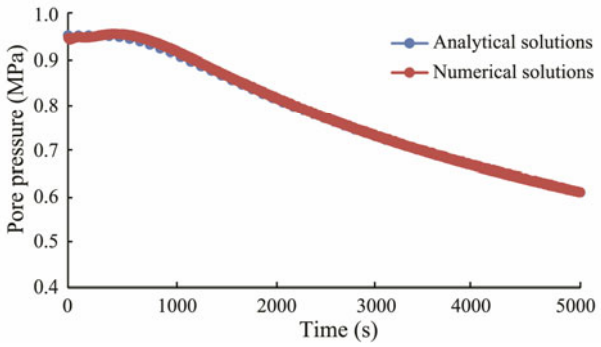

Fig.4 Comparison between analytical and numerical solutions of pore pressure at $z=25$m.

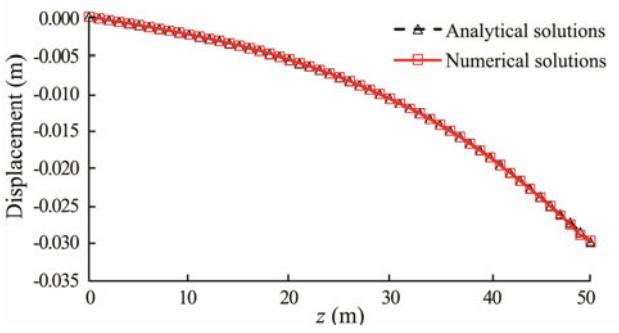

Fig.5 Comparison between analytical and numerical solutions of displacement profile at $t=5000$ s.

Fig.4 shows that the pore pressure increases to ap-

proximately 1 MPa due to the instantaneous load at the initial time. As time passes, the pore pressure of the soil at $z=25$ m dissipates gradually and decreases to 0.61 MPa at $t=5000$ s. Fig.5 shows the displacement profile at $t=5000$ s. The displacement at the top changes much faster than the displacement at the bottom because the pore pressure at the top dissipates more quickly. All the results indicate that the numerical solutions of pore pressure and displacement agree well with the analytical solutions, thereby validating the numerical model's accuracy.

5 Compaction Law of Shallow Sediments

For simplicity, the one-dimensional compaction model is used to analyze the compaction law of shallow sediments under their own weight. However, this approach is applicable only to the sedimentary basin with large horizontal extent. Thus, the deposition is fairly uniform over a large area whose dimensions are much larger compared with the thickness of the layer.

As shown in Fig.3, the sediment layer forms over an impermeable rigid basin floor due to the continuous deposition of solids at a constant rate. Displacements in the horizontal directions are fixed for laterally confined condition. The pore pressure at the top surface of the sediment is equal to the hydrostatic pressure at the seafloor. The pore fluid flow occurs along the vertical direction only. The sea level is located at $L=2000$ m.

The following material parameters of the sediment are used: initial dry density $\rho_{d0}=1200\,\mathrm{kg\,m^{-3}}$, initial void ratio $e_0=3$, initial permeability $k_0=0.5\times10^{-13}\,\mathrm{m^2}$, permeability index $b=3.8$, Poisson's ratio of 0.3, Biot's coefficient $\alpha=1$, slope of the normal consolidation line $\lambda=0.1$, 0.16, slope of the swelling line $\kappa=0.04$, frictional constant $M=0.57$, gravity acceleration $g=9.80\,\mathrm{m\,s^{-2}}$, deposition rate $\dot{m}=0.1\,\mathrm{mm\,yr^{-1}}$, sea water density of $\rho=1030\,\mathrm{kg\,m^{-3}}$, and dynamic viscosity of sea water $\mu=1$ mPa.s. The reference pressure p_1 is taken to be the effective vertical stress near the seafloor. Here, we set $p_1=14700$ Pa (1 m below the seafloor). The initial pre-consolidation pressure is set to be equal to p_1. The thickness of each element is 0.1 m and is small enough to capture the dynamic process of the deposition by testing.

5.1 Change in Thickness of the Sediment Layer Over Time

To evaluate the effect of material parameters on the compaction law, two simulations are performed for two values of the slope of the normal consolidation line, namely, $\lambda=0.10$ and 0.16. The duration time of deposition is 10 million years (Ma). When time >10 Ma, the deposition stops. The numerical results of the thickness of the sediment layer over time are shown in Fig.6. To observe the difference between the large and small strain models, the results obtained from the small strain model are also given.

Fig.6 illustrates that the thickness increases nearly linearly when $t<10$ Ma. The ultimate settlement of the sediments calculated from the small strain models is larger than that obtained from the large stain model. However, both models indicate that the deformation is large during compaction. Thus, the large strain model is more applicable for the problem of sediment compaction. However, the thickness at $t=10$ Ma is different for different λ. For the large strain model, the thickness at $t=10$ Ma is approximately 910 m when $\lambda=0.10$, while the thickness is 885 m for $\lambda=0.16$ because the sediment is more prone to compression for lower λ. After the deposition stops ($t>10$ Ma), the thickness decreases with time slowly due to the dissipation of pore pressure. As time passes, the thickness decreases more slowly and finally becomes stable. The final thickness depends on the deformation parameters of the sediment, which are 743 m and 611 m for $\lambda=0.10$ and 0.16, respectively.

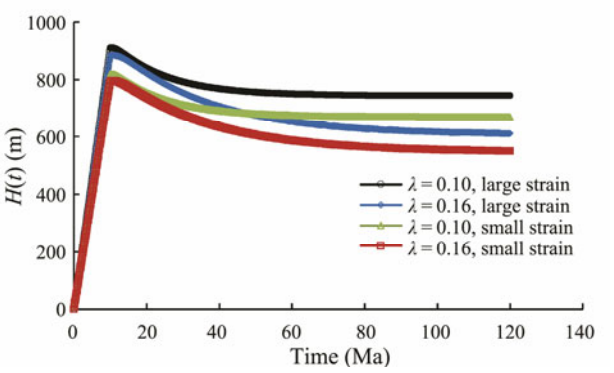

Fig.6 Change in thickness of the sediment over time.

5.2 Pore Pressure Profile Over Time

The prediction of the pore overpressures induced by rapid deposition is of great practical importance in oil drilling operations, especially for deepwater drilling program. The evolution of pore pressure profile for $\lambda=0.16$ is shown in Fig.7.

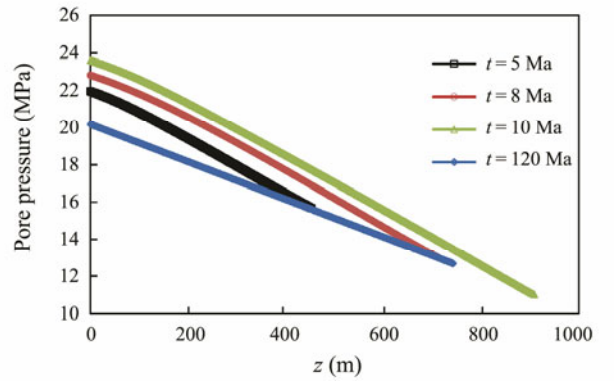

Fig.7 Evolution of pore pressure profile.

During the deposition, the sediment becomes dense under the weight of continuous material supply. Thus, the pore pressure increases continually over time due to the rapid decrease in pore space. When $t=10$ Ma, the pressure variation at the base ($z=0$ m) is approximately 3.4 MPa

compared with the hydrostatic pressure. After the deposition stops ($t>10$ Ma), the weight of the sediment remains unchanged. The pore pressure stops increasing and starts to dissipate until the pore pressure reverts to the hydrostatic pressure state. If the deposition does not stop, then the pore pressure will increase continually despite the permeability and the deposition rate of the sediment. This issue will be discussed in detail in the following section.

5.3 Displacement and Void Ratio Profile Over Time

Engineering mechanical properties are the fundamental parameters for the design of the driving depth of a riser, the setup of a wellhead, and drilling fluid because many engineering properties of shallow layers (such as undrained shear strength and permeability) are related closely to the void ratio. The prediction of void ratio profile is important during deepwater shallow layer drilling. Figs.8 and 9 show the evolution of displacement and void ratio profile at different times.

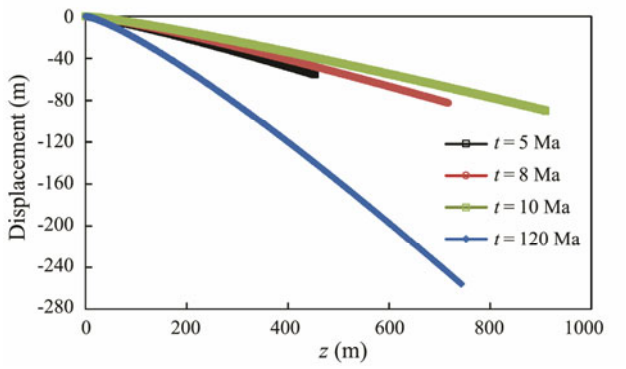

Fig.8 Evolution of displacement profile at different times.

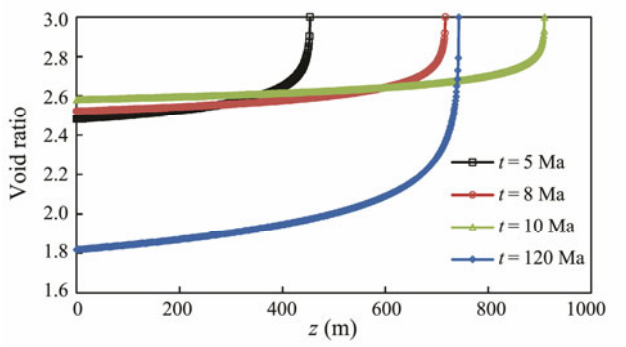

Fig.9 Evolution of void ratio profile at different times.

Fig.8 shows the change in displacement profile over time; the displacement increases as the depth increases. Although the settlement of the sediment top face increases over time (55, 82, and 90 m for $t=5$, 8 and 10 Ma) when $t<10$ Ma, the thickness of the sediment increases with time due to continuous deposition. After the deposition stops, the settlement of the top surface increases because of the gradual dissipation of pore pressure. The eventual settlement is 256 m when $t=120$ Ma.

Fig.9 shows the change in void ratio profile over time. The void ratio decreases strictly with depth and decreases more quickly near the seafloor than in the deeper layer. An interesting phenomenon is that the void ratio in the deeper layer increases over time when $t<10$ Ma because the pore pressure increases due to the rapid deposition of sediment. The effective stress is reduced, thereby leading to the slow deformation of the sediment. When the deposition stops ($t>10$ Ma), the void ratio decreases again and becomes 1.8 near the basement for $\lambda=0.16$ when $t=120$ Ma.

5.4 Effect of Vertical Heterogeneity on Compaction

The deposits at different geological period are usually different, thereby causing a difference in mechanical property at different burial depths. This situation is common in deepwater shallow formation. To evaluate the effect of vertical heterogeneity on compaction law, three layers with different properties are considered in the model. The thickness of these layers are 200, 300, and 500 m, respectively, and the corresponding dry densities are 1200, 1300, 1250 kg m^{-3}, respectively. λ in each layer is uniform and is 0.16, 0.12, and 0.14, respectively. Fig.10 shows a comparison between void ratio profiles of the heterogeneous and homogeneous formations ($\lambda=0.16$, $\rho_{d0}=1200$ kg m^{-3}) when $t=120$ Ma.

As shown in Fig.10, when the formation is homogeneous, the void ratio decreases as the depth increases. However, when the formation is heterogeneous, a jump occurs at the interface of the different layers. This finding indicates that the void ratio in the heterogeneous formation does not always decrease with the increase in depth even though no overpressure formation exists. This finding is a notable point when predicting the pore pressure with the normal compaction curve method.

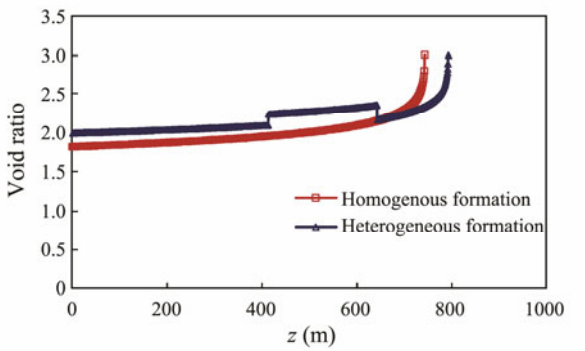

Fig.10 Comparison of void ratio profile between homogeneous and heterogeneous formations.

6 Numerical Simulation of Overpressure Evolution of Shallow Water Flow Sands Under Compaction

SWF sands are shallow sands with overpressure and usually exist in a deepwater area. The sands are unconsolidated and have high porosity and permeability. Abnormally pressured sands are usually found at shallow depths (usually several hundreds of meters) and are a primary geological hazard to deepwater drilling program

in many deepwater areas, such as the Gulf of Mexico and West Africa. More than 60% of all deepwater wells in the Gulf of Mexico have experienced SWFs (O'Leary *et al*., 2004). Drilling shallow overpressured sands may cause large and long-lasting uncontrolled flows, borehole instability, and foundation failure. SWF zones also impede logging and re-entry in open hole and the setting of cement behind casing.

The generation mechanism of abnormal high pressure in shallow sands is a complicated geological process. Numerous factors, such as sedimentary compaction, tectonic movement, and submarine landslide, contribute to the generation of high pore pressure. Given the shallow burial depth of SWF sands, the compaction due to rapid compaction is usually considered the main mechanism generation of high pore pressure. The one- and two-dimensional compaction models are used to study the evolution law of overpressure of SWF sands. The one-dimensional compaction model is used to study the governing factors of generation of SWF due to the under-compaction of sediment, and the two-dimensional compaction model is used to study the differential compaction effect on the generation of overpressure.

6.1 Governing Factors of Overpressure Generation in SWF Sands

Fig.11 shows a schematic of one-dimensional compaction of SWF sands. The thickness of the existing sediment is 300 m. The distance between the sea level and the basement is 3000 m.

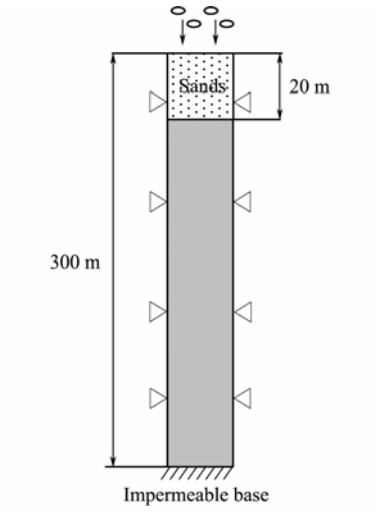

Fig.11 Schematic of one-dimensional compaction of SWF sands.

The sandy body with a thickness of 20 m is located at the top of the sediment surface. Before the subsequent deposition of clays, the existing sediment has already reached the normal compaction state. Similar to the situation described in the one-dimensional model, the sediment layer forms over an impermeable rigid basin floor due to the continuous deposition of solids at a constant rate. Displacements in the horizontal directions are fixed for the laterally confined condition. The pore pressure at the top surface of the sediment is equal to the hydrostatic pressure at the seafloor. The pore fluid flow occurs along the vertical direction only.

The modified Cam-Clay model is used to describe the deformation of clay sediment, while the Mohr-Coulomb model is used to describe the elastic and plastic deformation of SWF sands. The material properties of clay sediment are the same as in above example. The properties for SWF sands are given as follows: void ratio $e=3$, permeability $k=5\times10^{-12}\,\mathrm{m}^2$ (5 Darcy), dry mass density $\rho_d=1500\,\mathrm{kg\,m^{-3}}$, elastic modulus $E=0.5\times10^{-8}$ Pa, Poisson's ratio $v=0.2$, cohesion $c=0.1$ MPa, and friction angle $\varphi=30^\circ$. The evolution of pressure of SWF sands with time under different clay permeabilities around the sands and deposition rate is analyzed.

The value of overpressure ΔP is used to evaluate the degree of abnormal pore pressure. ΔP is calculated as

$$\Delta P = P - P_n\,, \tag{34}$$

where ΔP is the value of overpressure, P is the pore pressure, and P_n is the hydrostatic pressure.

The evolution of overpressure of sands for different overlying clay initial permeabilities at different deposition rates (0.2, 0.7, and 1.2 $\mathrm{mm\,yr^{-1}}$) over time in the sands is plotted in Figs.12, 13, and 14.

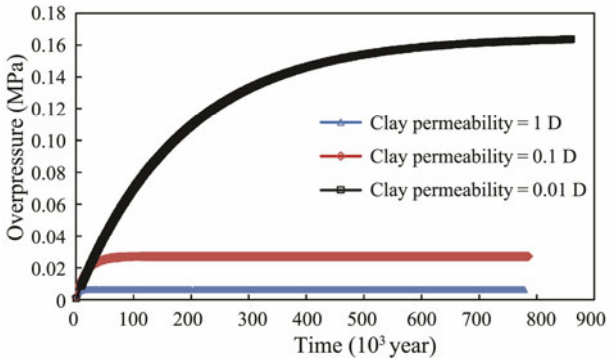

Fig.12 Evolution of overpressure for different overlying clay initial permeabilities when the deposition rate is 0.2 $\mathrm{mm\,yr^{-1}}$.

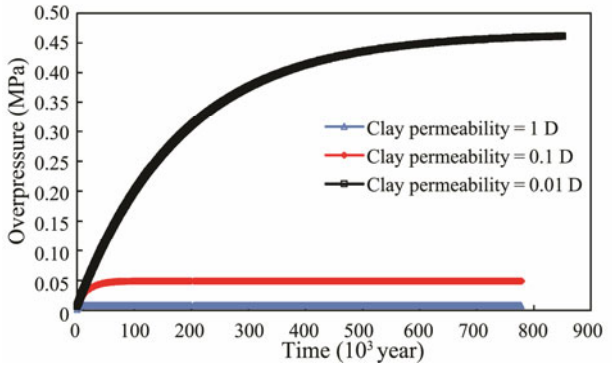

Fig.13 Evolution of overpressure for different overlying clay initial permeabilities when the deposition rate is 0.7 $\mathrm{mm\,yr^{-1}}$.

Figs.12, 13, and 14 show that the generation of over-

pressure of SWF sands is related closely to the initial permeability k_0 of the overlying clays. The value of overpressure increases with the decrease in the permeability of the overlying clays. For example, when the deposition rate is 0.2 mm yr^{-1}, the maximum overpressure of sands is merely 0.006 MPa when k_0=1 Darcy. The degree of overpressure is extremely slight in this case, while the values of overpressure are 0.027 and 0.163 MPa for k_0=0.1 and 0.01 Darcy, respectively. The results show that the low permeability of the overlying clay is an essential factor for the generation of high pressure in SWF sands. From the above calculation results, we can conclude that the overpressure of the sand has an upper limit. When the overpressure reaches this limit, then the expulsion of pore water and the deposition of sediment have achieved the dynamic equilibrium state.

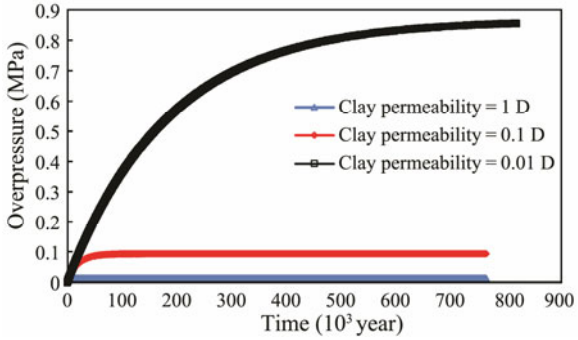

Fig.14 Evolution of overpressure for different overlying clay initial permeabilities when the deposition rate is 1.2 mm yr^{-1}.

A comparison of Figs.12, 13, and 14 shows that the deposition rate also affects the degree of overpressure of the SWF sands considerably. For example, the maximum overpressure of sands for different deposition rates (0.2, 0.7, and 1.2 mm yr^{-1}) are 0.16, 0.46, and 0.86 MPa, respectively, which is a result of two effects. One effect is the reduction in the void ratio of overlying clay at faster deposition rates, thereby decreasing the permeability and impeding the expulsion of pore water out of the sands as a result. Another effect is that the rapid deposition of sediment leads to the reduction of the pore space in the sands, thereby increasing pore pressure. For convenience of comparison, the overpressure evolution at different deposition rates when k_0=0.01 Darcy is plotted in Fig.15.

6.2 Numerical Simulation of Overpressure Evolution of SWF Sands Due to Differential Compaction

The different deposition rates at different regions lead to varying thickness in these different regions. Consequently, the overburden pressure of the sediments with a larger thickness is higher than that of the sediments with a smaller thickness. According to the above numerical results, the rapid deposition rate leads to higher overpressure in the thicker sediment. Then, the pore fluid starts to flow from the region with a higher pore pressure to the region with a lower pressure. This condition is called differential compaction and is a possible reason for the generation of overpressure in SWF sands.

The two-dimensional compaction model is used to analyze the overpressure evolution of SWF sands due to differential compaction. Fig.16 shows a schematic of the model.

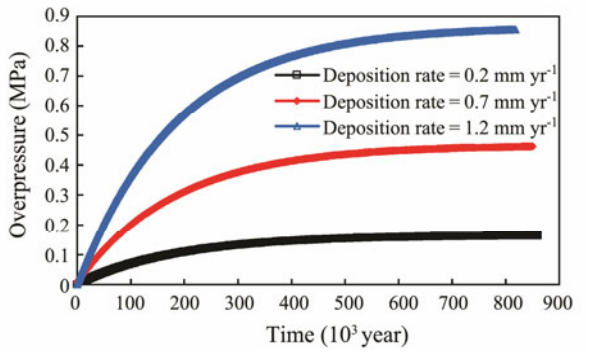

Fig.15 Evolution of overpressure for different deposition rates when the overlying clay initial permeability is 0.01 D.

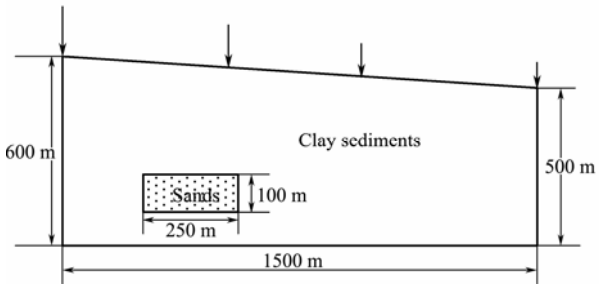

Fig.16 Schematic of two-dimensional compaction model.

The deposition rate decreases from left (1 mm yr^{-1}) to right (0.2 mm yr^{-1}) in Fig.15, thereby resulting in a trapezoid-shaped geometry. The sediment layer forms over an impermeable rigid basement. The distance between the basement and the seal level is 3000 m. Before the subsequent deposition of clays, the existing sediment has already reached the normal compaction state. The horizontal displacements at the left and right boundaries are fixed and fluid flow is not allowed at the left and right boundaries. The pore pressure at the top surface of the sediment is equal to the hydrostatic pressure at the seafloor. The material properties of the clay sediments and sands are the same as in the above numerical examples.

To accelerate the calculation speed (because of the low efficiency of the deactivation/reactivation method for the two-dimensional problem), we applied vertical pressure on the top surface of the geometrical model at different loading rates to simulate the different deposition rates instead of using the deactivation/reactivation method. The loading rate is set to be equal to the increased weight per time step. Thus, the loading rates are 19.3 and 3.9 Pa yr^{-1} at the left and right boundaries, respectively. The deposition period is 0.24 million years, and the deposition was interrupted when t>0.24 Ma. Fig.17 shows a comparison of the overpressure of the sands at the center point and the neighboring clay sediment at the left side of the sands over time.

When $t<0.24$ Ma, the overpressure increases over time in both sands and the neighboring clay sediment. However, the overpressure of the sands continues to increase, while the overpressure of the clay sediment starts to decrease when the deposition stops ($t>0.24$ Ma). The possible reason for the difference is that the fluid in the clay sediment flows into the sands. To prove this concept, the flow velocity vectors at $t=0.30$ Ma are plotted in Fig.18. The fluid in the clay sediment around the SWF sands flows into the sands, thereby increasing the pore pressure in the sands. This condition explains that the mechanism of differential compaction affects the generation of abnormal pressure in SWF sands.

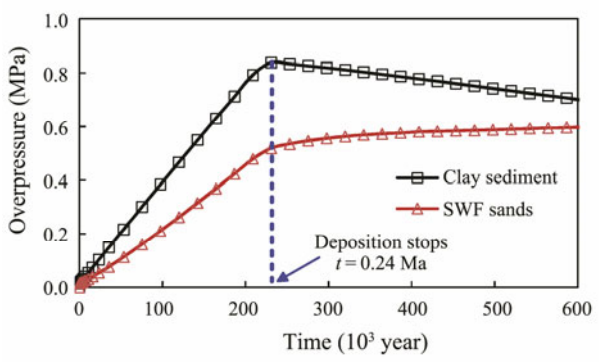

Fig.17 Comparison of overpressure evolution between the sands and the neighboring clay.

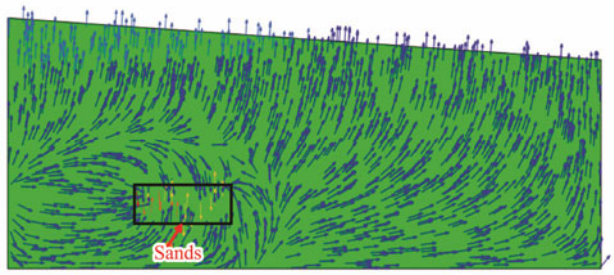

Fig.18 Fluid flow field at $t=0.30$ Ma.

7 Conclusions

A compaction model of the shallow sediments in the deepwater region is formulated, taking geometry and material nonlinearity into consideration. The moving top boundary of the sediments is simulated by the deactivation/reactivation method. The modified Cam-Clay model is selected as the constitutive model of the clay sediments. This model can account for the hardening law of the material induced by volumetric strain change. An explicit finite difference method using FLAC^{3D} is applied to solve the compaction model, which is proven to be applicable for the large deformation and nonlinear problem.

The compaction law of shallow sediment over time is analyzed by using the one-dimensional compaction model. Findings indicate that the final settlement of the shallow sediments is large due to the large deformation driven by their own weight. Therefore, large strain analysis is needed for the compaction of shallow sediment. The void ratio profile shows that the void ratio decreases greatly with the burial depth when the formation is homogeneous and decreases more quickly near the seafloor than in the deeper layer. When the heterogeneity is considered, the void ratio jumps at the interface of the different layers. The evolution of pore pressure profile indicates that the pore pressure increases with time due to the continuous deposition of sediments. When the deposition is interrupted, the pore pressure starts to dissipate and finally reaches the hydrostatic state.

SWF is a general geological hazard encountered in deepwater drilling programs. The compaction law of the shallow sediment is considered a principal mechanism for the generation mechanism of abnormal pressure in the SWF sands. One-dimensional numerical simulation results show that the main factors that have an important influence on the displacement are deposition rate and permeability of the overlying clay sediment. Overpressure increases with an increase in deposition rate and a decrease in the permeability of the overlying clay sediment. Moreover, an upper limit exists for the overpressure of the SWF sands at a constant deposition rate. A two-dimensional model is used to study the effect of differential compaction on the generation of overpressure in the SWF sands. The results show that the pore pressure still increases due to the inflow of the pore fluid from the neighboring clay sediment even though the deposition process is interrupted. The numerical model presented in this paper provides a fundamental understanding of the compaction law of deepwater shallow sediments. Further study is required to improve the efficiency and accuracy of the method. Actual geological and experimental data are also needed to validate the model.

Acknowledgement

This study was funded by the National Key Basic Research Program of China (973 Program) (No. 2015 CB25 1201), NSFC-Shandong Joint Fund for Marine Science Research Centers (No. U1606401), and Key Science & Technology Foundation of Sanya (Nos. 2017PT13 and 2017PT14).

References

Athy, L. F., 1930. Density, porosity, and compaction of sedimentary rocks. *AAPG Bulletin*, **14** (1): 1-24.

Audet, D. M., and Fowler, A. C., 1992. A mathematical model for compaction in sedimentary basins. *Geophysical Journal International*, **110** (3): 577-590.

Bachrach, R., 2016. Mechanical compaction in heterogeneous clastic formations from plastic-poroelastic deformation principles: Theory and applications. *Geophysical Prospecting*, **65**: 724-735.

Bernaud, D., Dormieux, L., and Maghous, S., 2006. A constitutive and numerical model for mechanical compaction in sedimentary basins. *Computers and Geotechnics*, **33** (6): 316-329.

Biot, M. A., 1941. General theory of three-dimensional consolidation. *Journal of Applied Physics*, **12** (2): 155-164.

Carter, J. P., Small, J. C., and Booker, J. R., 1977. A theory of finite elastic consolidation. *International Journal of Solids and Structures*, **13** (5): 467-478.

Chopra, M. B., and Dargush, G. F., 1992. Finite-element analysis of time-dependent large-deformation problems. *International Journal for Numerical and Analytical Methods in Geomechanics*, **16** (2): 101-130.

Davis, E. H., and Raymond, G. P., 1965. A non-linear theory of consolidation. *Geotechnique*, **15** (2): 161-173.

Detournay, E., and Cheng, A. H. D., 1993. Fundamentals of poroelasticity. In: *Comprehensive Rock Engineering*: *Principles*, *Practice & Projects*. Pergamon Press, Oxford, 90-95.

Fowler, A. C., and Yang, X. S., 1998. Fast and slow compaction in sedimentary basins. *SIAM Journal on Applied Mathematics*, **59** (1): 365-385.

Gherasim, M., Viceer, S., Brusova, O., and Naumenko, J., 2015. Application of an integrated workflow for shallow-hazard characterization using a 3D high-resolution survey offshore Azerbaijan. *The Leading Edge*, **34** (4): 390-396.

Gibson, R. E., 1958. The progress of consolidation in a clay layer increasing in thickness with time. *Geotechnique*, **8** (4): 171-182.

Gibson, R. E., England, G. L., and Hussey, M. J. L., 1967. The Theory of one-dimensional consolidation of saturated clays: 1. finite non-Linear consildation of thin homogeneous layers. *Geotechnique*, **17** (3): 261-273.

Haneberg, W. C., Kelly, J. T., Graves, H. L., and Dan, G., 2015. A GIS-based decision-support approach to deepwater drilling-hazard maps. *The Leading Edge*, **34** (4): 398-404.

Hedberg, H. D., 1936. Gravitational compaction of clays and shales. *American Journal of Science*, **5** (31): 241-287.

Kikinzon, E., Kuznetsov, Y., Maliassov, S., and Sumant, P., 2015. Modeling fluid flow and compaction in sedimentary basins using mixed finite elements. *Computational Geosciences*, **19** (2): 285-298.

Mallick, S., and Dutta, N. C., 2002. Shallow water flow prediction using prestack waveform inversion of conventional 3D seismic data and rock modeling. *The Leading Edge*, **21** (7): 675-680.

Nygård, R., Gutierrez, M., Gautam, R., and Hoeg, K., 2004. Compaction behavior of argillaceous sediments as function of diagenesis. *Marine and Petroleum Geology*, **21** (3): 349-362.

O'Leary, J., Flores, J. C., Rubinstein, P., and Garrison, G., 2004. Cementing deepwater, low-temperature Gulf of Mexico formations prone to shallow flows. *IADC/SPE Drilling Conference*. Dallas, USA, 1-11.

Skogdalen, J. E., Utne, I. B., and Vinnem, J. E., 2011. Developing safety indicators for preventing offshore oil and gas deepwater drilling blowouts. *Safety Science*, **49** (8): 1187-1199.

Sun, B. J., and Zhang, Z. N., 2015. Challenges and Countermeasures for the drilling and completion of deepwater wells in the South China Sea. *Petroleum Drilling Techniques*, **43** (4): 1-7 (in Chinese with English abstract).

Sun, J., Deng, J., Yu, B. H., and Peng, C. Y., 2015. Model for fracture initiation and propagation pressure calculation in poorly consolidated sandstone during waterflooding. *Journal of Natural Gas Science and Engineering*, **22**: 279-291.

Sun, Y., Zhao, T., and Qin, K., 2014. Numerical simulation of overpressure of shallow water flow in Baiyun Sag of the northern South China Sea. *Advances in Earth Science*, **29** (9): 1055-1064 (in Chinese with English abstract).

Xie, K. H., and Leo, C. J., 2004. Analytical solutions of one-dimensional large strain consolidation of saturated and homogeneous clays. *Computers and Geotechnics*, **31** (4): 301-314.

Xie, X. Y., Huang, J. Q., Wang, W. J., and Lin, J. Z., 2014. Influence of weight of soils on nonlinear finite strain consolidation for Ningbo soft clay. *Journal of Zhejiang University (Engineering Science Edition)*, **48** (5): 827-834 (in Chinese with English abstract).

Xie, Y. H., 2014. A major breakthrough in deepwater natural gas exploration in a self-run oil/gas field in the northern South China Sea and its enlightenment. *Natural Gas Industry*, **34** (10): 1-8 (in Chinese with English abstract).

(Edited by Chen Wenwen)